ISSN (Online) 2456-1290

International Journal of Engineering Research in Mechanical and Civil Engineering (IJERMCE)

Volume 11, Issue 7, July 2024

Assessment of the Stress Instability Workability Criterion for Internal Ductile Failure in Three-Stage Steel Cold Heading Process

Amar Sabih

Concordia University, Montreal, Canada &
McGill University, Montreal, Canada

Email: amar.sabih@concordia.ca & amar.sabih@mcgill.ca

***Abstract*— The cold heading process is a multistage process which is performed without an external heat source. The occurrence of internal ductile failure in cold-headed products is caused by the adiabatic shear band phenomenon. This type of failure presents a significant obstacle in the fast-expanding cold heading industry. The existence of these types of ductile failure in cold-headed products may lead to catastrophic fracture under tensile loads despite the ductile nature of the material.**

The current work presents a comprehensive experimental and finite element methodology to implement the stress instability workability criterion in assessing and improving multistage cold heading procedures.

The new methodology showed that it is an efficient tool to predict the damage levels and failure initiation locations within cold-headed products. Moreover, this methodology is successful in optimizing the die designs to reduce damage levels.

***Index Terms*— Adiabatic Shear Band, Stress Instability, Cold Heading, Multistage Process, Ductile Failure, Workability Criterion**

I. INTRODUCTION

The cold-heading (CH) process is a complex procedure in which the quality of the cold-headed product depends on various material and process parameters. Currently, the design of cold-headed products is based on empirical, and trial and error rules developed over many years. However, these traditional rules are not sufficient for designing CH processes to produce defect-free products under higher strains and strain rates.

Sabih and Nemes [1] conducted an experimental and finite element analysis study, which demonstrated that increasing the CH strain rates and strains leads to internal failure caused by the adiabatic shear band (ASB) phenomenon. The study confirmed that ASBs develop through complicated stages leading to a sudden drop in flow stress triggered by the stress instability phenomenon.

Several researchers, including Clifton [2], Bai [3], Merzer [4], Wright and Batra [5], and Sabih and Nemes [6], observed that as strain increases, stress reaches a maximum value and then slowly decreases, followed by a rapid collapse. Sabih and Nemes [6] proved that this critical stage is caused by the stress instability phenomenon, leading to localization and eventually ductile failure. Based on this finding, Sabih and Nemes [6] used this phenomenon to develop a new workability criterion to predict ductile failure in the cold heading process.

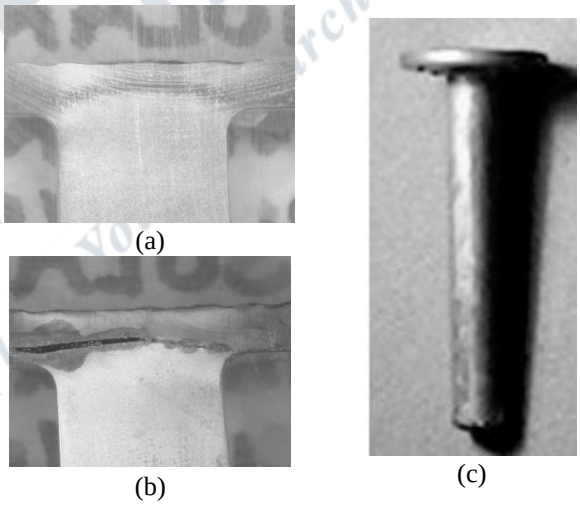

Fig. 1 Sectioned bolts revealing material flow inside the bolt head after etching with Fry's reagent (cupric chloride 36g; 145ml hydrochloric acid; 80 ml water): (a) without internal defect, (b) with defect bolt caused by ASB phenomenon. (c) Original bolt before sectioning

The following sections will provide details about the types of ASBs, their stages, and the associated failure. This will be followed by the experimental and finite element (FE) modeling procedure used to study the ASB phenomenon, developing the stress instability workability limits. The final part of this paper focuses on using these limits in assessing three staged cold heading designs followed by the conclusions if this work.

ISSN (Online) 2456-1290

International Journal of Engineering Research in Mechanical and Civil Engineering (IJERMCE)

Volume 11, Issue 7, July 2024

1.1 Adiabatic Shear Band (ASB) phenomenon

Meyers and Wittman [7] defined the adiabatic shear band (ASB) as shear bands that form at strain rates higher than 10^2 s^{-1}. The term "adiabatic" is used because heat generation during deformation is much higher than heat loss. Klepaczko and Rezaig [8] found that these bands can be several millimeters or centimeters long, but only a few tens of microns thick. The highly strained material within the ASB maintains physical continuity from one side to the other.

In cold-headed parts, the ASB phenomenon is primarily controlled by thermal and mechanical factors. It typically occurs under impact loading at high strain rates and high strains. Initially, the work hardening mechanism dominates, leading to an increase in flow stress. However, 90–95% of the plastic work is converted into heat, resulting in a local temperature increase and a decrease in flow stress. This creates a competition between work hardening and thermal softening in the deformation zone [8]. If the material deformation continues, the thermal softening mechanism eventually dominates, causing unstable deformation. Nabil Basim [9] noted that this instability leads to deformation localizing into a narrower band, resulting in internal failure in cold-formed parts, as shown in Fig. 1. Therefore, it is crucial to understand the different stages of the ASB phenomenon, especially the instability phenomenon, to gain a better understanding of the failure mechanism in cold-headed parts.

Marchand and Duffy [10] performed an intensive investigation of the initiation and propagation of ASBs in low alloy steel (HY-100) using the Kolsky bar torsion test and still cameras. This study proved that ASBs develop in three stages:

Stage I: The band will go through homogeneous plastic strain with an increase in flow stress.

Stage II: The second stage starts when the strain distribution becomes inhomogeneous. During this stage, the flow stress will continue to increase while the deformation proceeds accompanied by a decrease in the ASB width. A sudden drop in flow stress will mark the end of stage II and the beginning of stage III of ASB development.

Stage III: The sudden drop in flow stress triggered by the instability phenomenon is accompanied by an increase in nominal strains and a decrease in ASB width. The situation in this stage is very critical as the material flow is unstable and strain localization takes place inside the band.

1.2 Instability Criterion

The onset of instability or strain localization within the ASBs, followed by the stress collapse, is an important factor in the development of ASB stages as it accelerates the deformation, leading to a fast ductile failure [10,11,12, 13].

A new workability criterion has been developed by Sabih and Nemes [6] to predict the limits for internal ductile failure in cold-headed steel parts. This criterion is based on a comprehensive experimental and finite element simulation methodology, including the drop weight compression test (DWCT) and finite element analyses using ABAQUS/Explicit. The criterion uses the ratio between equivalent stress at instability and failure to reveal the initiation of internal ductile failures.

For these failed locations, the $\bar{\varepsilon}_p^f$ and the ratio $(\bar{\sigma}_{failure}/\bar{\sigma}_{instability})$ values were calculated from the FE simulations of the corresponding specimens.

The relationship between $(\bar{\sigma}_{failure}/\bar{\sigma}_{instability})$and $\bar{\varepsilon}_p^f$ was plotted for all failed locations to calculate the material constants A and C.

$$\bar{\varepsilon}_p^f = C + A\left(\bar{\sigma}_{failure}/\bar{\sigma}_{instability}\right) \qquad (1)$$

The process to determine the material parameters for the workability criterion involves several steps outlined in Fig. 2. These steps primarily include the drop weight compression test (DWCT) to replicate the CH process alongside FE analysis conducted in ABAQUS/Explicit.

Metallographic inspection of the deformed specimens is carried out to identify the failed zones within the ASB. The results from both the experimental and FE simulations are utilized to determine the material constants C and A. In this study, the occurrence of internal cracks exceeding 100 µm in length along the ASB is considered as the measure of failure.

The main goal of this work is to present a comprehensive experimental and finite element methodology in assessing and improving multistage cold heading designs by implementing the stress instability workability criterion presented by Sabih and Nemes [6].

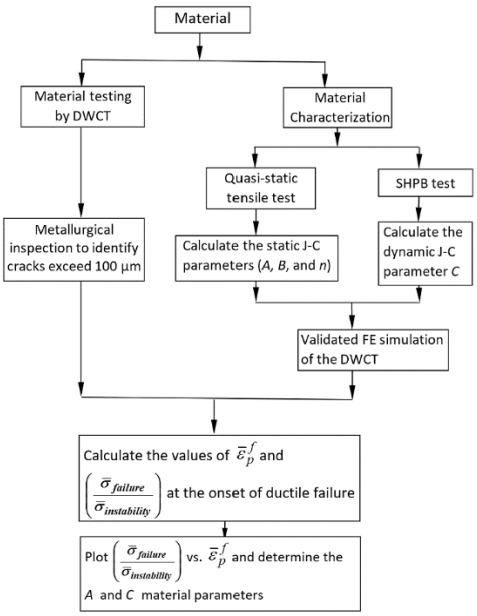

Fig. 2 The methodology used to determine the material parameters for the stress instability criterion

ISSN (Online) 2456-1290

International Journal of Engineering Research in Mechanical and Civil Engineering (IJERMCE)

Volume 11, Issue 7, July 2024

II. METHODOLOGY

A. Testing Materials

The CH quality AISI steel grades chosen for this research are 1008, and 1038 steel which represent low and medium carbon content steels. These materials were received in rod form from Ivaco Rolling Mills (Ontario, Canada). Table 1 presents the chemical composition of the three steels under study. In general, the microstructures consist of ferrite matrix and lamellar pearlite. The microstructure content of 1008 steel consists of 15% lamellar pearlite and 85% ferrite. Since the carbon content is the 1038 steel is higher; the microstructure of 1038 steel consists of 50% ferrite matrix and 50% lamellar pearlite.

Table1: Chemical Composition of the testing material (wt%)

AISI Steel grade	C	Mn	P	S	Si	Cu	Ni	Cr
1008	0.09	0.4	0.018	0.012	0.01	Nil	0.01	0.02
1038	0.38	0.82	0.007	0.002	0.19	0.04	0.08	0.08
AISI Steel grade	**Mo**	**Sn**	**Al**	**N**	**B**	**V**	**Co**	
1008	0.002	0.002	0.038	0.0046	-	-	0.004	
1038	0.001	0.003	0.003	0.0044	0.0001	0.005	-	

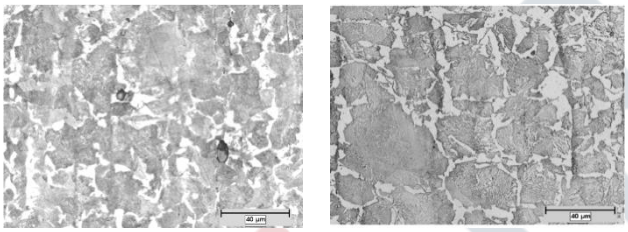

(a) **(b)**

Fig. 3 As-received testing materials microstructure: (a) 1018 steel, (b) 1038 steel

B. Drop Weight Compression Test (DWCT)

The DWCT as described by Nickoletopoulos [14] was used as a workability test to perform the cold heading of the specimens (Fig. 4). The DWCT facilitates the testing of the CH process, and it can generate internal cracks during upset testing. The DWCT machine (Fig. 4-a) consists of a tower enabling interchangeable weight plates to be dropped from heights up to 2.4 m. The die set configuration (Fig. 4-b) rests on a central column that is welded to the base of the DWCT machine. Specimens for CH were machined with a tolerance of 0.02 mm from as-rolled rod material to a cylindrical configuration of 5.3 mm in diameter with aspect ratios of 1.6 and 1.8. A series of tests is performed by varying the weights until the internal fracture is determined.

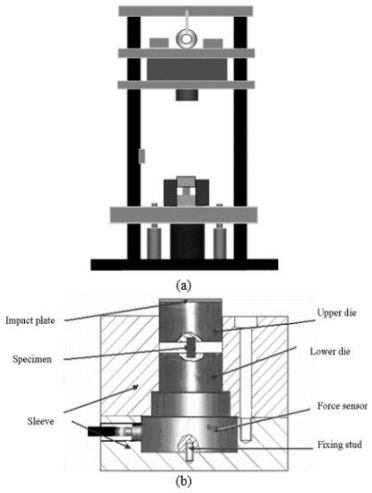

Fig. 4 (a) Schematic of the DWCT machine and (b) the specimen in the DWCT die arrangement

C. FE Simulation and Constitutive Model

The FE model implemented with ABAQUS/Explicit has been used to simulate the DWCT for the current work. The Johnson-Cook model (J-C) [15] is used to describe the thermo-plastic, rate-dependent behaviour of the material in a two-dimensional, axisymmetric, adiabatic, analysis of a cylindrical specimen under impact loading. The meshing of the specimen is performed using 4-noded continuum elements with reduced integration and hourglass control (CAX4R).

Accurate ASB modelling under high strain rate deformation processes over a wide range of strain rates and temperature changes requires reliable constitutive modelling of the stress–strain behaviour. This enables the prediction of flow stress collapse at the onset of the instability phenomenon during ASB development. The concept of stress collapse in adiabatic shear bands has been discussed in detail by Wright and Walter [16] who concluded that the stress drops and the onset of the instability phenomenon during high strain rate deformation is of greater importance than the localization of deformation.

The Johnson-Cook [15] model is used in the FE simulations of the current work because it provides a

good prediction for high-rate deformation mechanical behaviour. This model is applied extensively for computational purposes because it also contains parameters that are easy to determine. The J-C model has been successful in modelling the ASB phenomenon (see the works of Meyers et al. [17]; and Johnson and Holmquist [18]. This success is related to the model's ability to correctly predict the onset of strain instability marked by flow stress collapse during ASB development.

In the Johnson-Cook model, the Von-Mises flow stress is represented by a multiplicative relation as follows:

ISSN (Online) 2456-1290

International Journal of Engineering Research in Mechanical and Civil Engineering (IJERMCE)

Volume 11, Issue 7, July 2024

$$\bar{\sigma} = (A + B\bar{\varepsilon}_p{}^n)(1 + C\, ln\frac{\dot{\bar{\varepsilon}}_p}{\dot{\bar{\varepsilon}}_o})(1 - T*^m) \quad (2)$$

Where $\bar{\sigma}, \bar{\varepsilon}_p$ and $\dot{\bar{\varepsilon}}_p$ are the effective flow stress, the effective plastic strain, and the effective plastic strain rate respectively. $\dot{\bar{\varepsilon}}_o$ is normally taken to be 1.0 s^{-1}. *A*, *B*, *n*, *C*, and *m* are material constants and *T** is the normalized temperature. The first term characterizes the strain hardening, whilst the second part accounts for strain rate dependence, and the last term captures the temperature effects.

The Split Hopkinson Pressure Bar (SHPB) is used to determine material response when subjected to deformation at high strain rates. Developed by Kolsky [19], the SHPB test has subsequently been used as a dependable method for determining the material behavior at high strain rates that cannot be reached by traditional equipment such as hydraulic or screw-driven testing machines. Several SHPB tests were conducted on 5x5 mm cylinders to determine the dynamic J-C parameter (C).

Table 2. The final J-C parameters for both testing materials

	Quasi-static parameters			Dynamic parameters	
Material	***A (MPa)***	***B (MPa)***	***n***	***C***	***m***
1008 steel	440	689	0.678	0.003	1
1038 steel	420	1528	0.440	0.082	1

On the other hand, the quasi-static tensile tests were performed on standard specimens to determine the J-C static parameters (A, B and n). The thermal softening constant, m, was set at 1, which has been reported to be a good approximation for several metals [15].

On the other hand, quasi-static tensile tests were performed on standard specimens to determine the J-C static parameters (A, B and n). The thermal softening constant, m, was set at 1, which has been reported to be a good approximation for several metals [15].

This onset of localization occurs when an increase in the equivalent plastic strain results in a decrease in the equivalent stress. This can be indicated by the maximum value of the equivalent stress-equivalent plastic strain relation. This can be expressed as:

$$\frac{d\bar{\sigma}}{d\bar{\varepsilon}_p} \leq 0 \quad (3)$$

Taking the equivalent stress to be a function of equivalent plastic strain, the equivalent strain rate, and temperature, Equation 3 may be written as:

By applying this to the J-C model utilized in this work the following is obtained:

$$\frac{\boldsymbol{Bn(\bar{\varepsilon}_p)^{n-1}}}{\boldsymbol{A+B(\bar{\varepsilon}_p)^n}} + \frac{\boldsymbol{C/\dot{\bar{\varepsilon}}_p}}{\boldsymbol{1+C\,ln\frac{\dot{\bar{\varepsilon}}_p}{\dot{\bar{\varepsilon}}_o}}}\frac{\boldsymbol{d\dot{\bar{\varepsilon}}_p/dt}}{\boldsymbol{d\bar{\varepsilon}_p/dt}} + \frac{\boldsymbol{-mT^{*m-1}}}{\boldsymbol{(1-T^{*m})(T_m-T_o)}}\frac{\boldsymbol{dT/dt}}{\boldsymbol{d\bar{\varepsilon}_p/dt}} \leq \mathbf{0} \quad (4)$$

The first and second terms in this expression represent the strain hardening and the strain rate-hardening effect, respectively, while the third term represents the thermal softening effect. Equation 4 gives the conditions for the onset of instability and strain localization. One way to determine this is by using Equation 4, from which the strain hardening term, rate hardening term, and thermal softening terms are plotted at a location within the region of maximum strain. Here, all the required data was collected from the FE simulation results.

Fig. 5 indicates that the sum of the three terms becomes negative at an approximate equivalent plastic strain of 0.97 for the 1038 steel DWCT specimen.

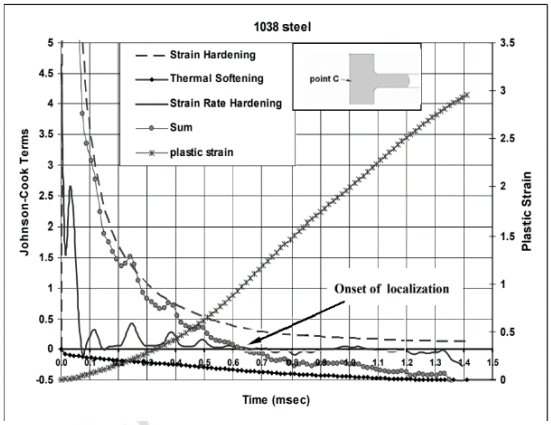

Fig. 5 Evaluation of hardening and softening terms, indicating the onset of localization at the center of the DWCT specimen at point C (1038 steel)

D. Assessment of the Multistage CH Designs

Before detailing the workability assessment process of the multistage CH designs used in this work, it is better to explain the goals, basis and definitions used in performing this assessment.

The workability methodology can be used to achieve two goals.

1. Choosing the CH material for a certain CH design: the workability methodologies can be used to select the CH materials that can produce a defect-free product that assure a maximum damage level within the acceptable limits indicated by these workability limits (Fig. 6).

2. Differentiating different CH designs: the workability methodologies can be used to differentiate between the different CH designs and indicate the best design that assures the lowest damage level in the final product in comparison with the other designs (Fig. 7). Moreover, it is possible employ these methodologies as a die optimization tool.

The assessment process is performed by determining maximum values of the damage indicator level with the aid of the FE simulation of the multistage CH designs.

ISSN (Online) 2456-1290

International Journal of Engineering Research in Mechanical and Civil Engineering (IJERMCE)

Volume 11, Issue 7, July 2024

III. RESULTS AND DISCUSSION

In general, microscopic and metallurgical examination of the DWCT specimens at different levels of deformation showed that voids and cracks that exceed 100 µm were found along the ASBs inside DWCT specimens (Fig. 8).

Finite element simulation runs were performed for the DWCT tests considering the different dropped weights used. Simulation results were used to study the changes in flow stress and equivalent plastic strain at different locations of the specimens. The sample of the finite element simulation results of the equivalent plastic strain and equivalent flow stress contours for a DWCT specimen are shown in Fig. 9.

The material constants of the ductile fracture criterion were determined according to the procedure explained earlier. The workability limits of 1008 and 1038 steels are shown in Fig 10.

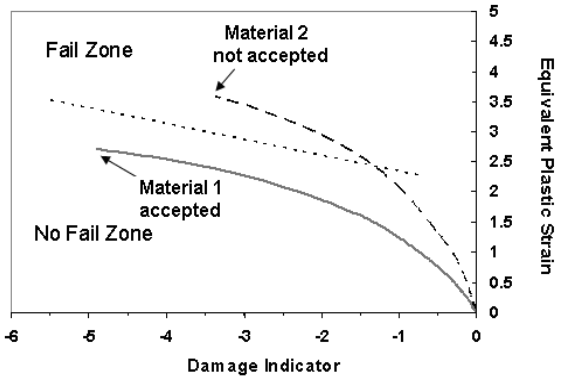

Fig. 6 Workability assessment of different CH materials.

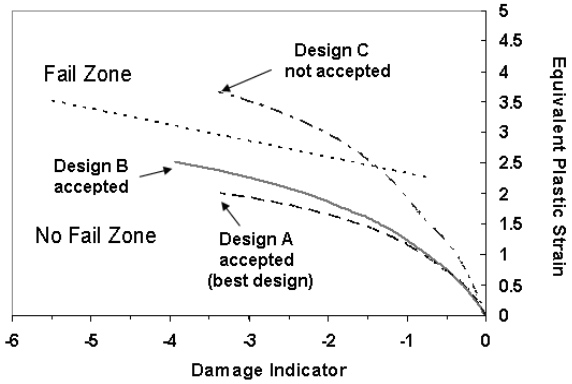

Fig. 7 Employing the workability methodologies in evaluating different CH designs

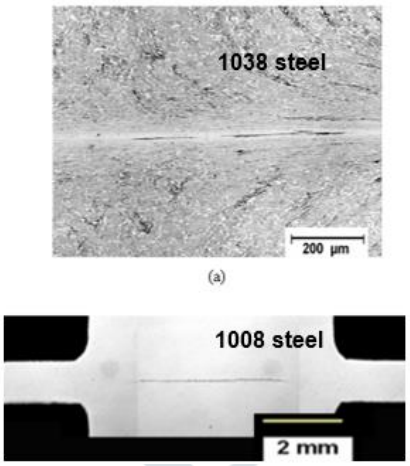

Fig. 8 Elongated cracks along a localized ASB in
(a) 1038 steel (aspect ratio= 1.8, drop height= 2.4 m, drop weight= 30.5 kg) (etchant: 2% Nital solution)
(b) 1008 steel (aspect ratio= 1.6, drop height= 2.4 m, drop weight= 37.6 kg)

Assessment of the Three-Stage CH Designs

Both three-stage designs (Fig. 11) use similar blanks and share identical third stage and lower dies. The first and second stages of these dies are different. Both designs are used to produce the same thin bolt head with a diameter approximately three times the size of the blank diameter in three stages. This process is a good example of a multistage CH process, as it requires careful material selection and CH design to produce a defect free product.

The ductile failure assessment procedure consists of using the J-C material parameters in the three-stage CH FE models. Thereafter, the FE simulations are used to determine the maximum values of the damage indicator parameter and the corresponding equivalent plastic strain. By comparing the damage indicator levels to the accepted damage limit, it is possible to indicate whether the damage levels in the finished cold-headed product are within the accepted limit or not.

The best way to explain the assessment procedure is to apply it to the same three-stage CH designs using two different CH heading materials, which result in acceptable and unacceptable final products, respectively. The materials selected for this purpose are 1008 steel and 1038 steel.

The FE simulation contours of the three-stage CH designs of 1008 steel shown in Fig. 12 revealed that a localized ASB initiated within the bolt head throughout the manufacturing stages of all materials. The equivalent stress contours reveal that the equivalent stress reached its maximum value followed by a drop marking the onset of the localization stage (Fig. 12-d). The localized ASB region experienced the highest plastic strain and lowest equivalent plastic tress (Fig. 12).

ISSN (Online) 2456-1290

International Journal of Engineering Research in Mechanical and Civil Engineering (IJERMCE)

Volume 11, Issue 7, July 2024

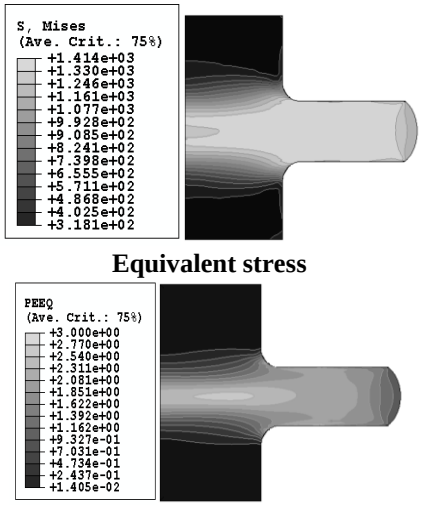

Equivalent stress

Equivalent plastic strain

Fig. 9 Finite element contours: (a) equivalent plastic strain; and (b) Equivalent flow stress

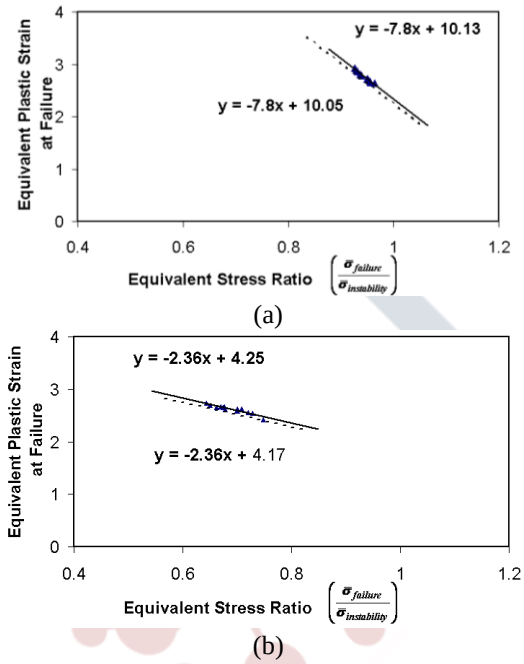

Fig. 10 The workability limits of the internal ductile failure in the CH process using the stress instability criterion: (a) 1008 steel, (b) 1038 steel. The solid line is the trend line of all failed points, and the broken line presents the safe workability limits

Using the FE simulation results of Design 1 and Design 2 three-stage CH process, the maximum ductile damage indicators were determined and plotted on the workability limits graphs. The resulting ductile failure workability assessment graphs are presented in Fig. 13 for 1008 steel and 1038 steel.

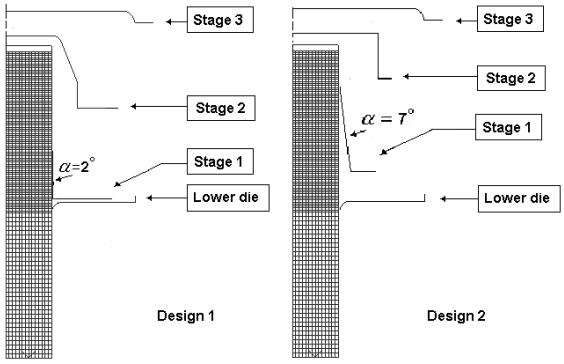

Fig. 11 A schematic of the three-stage CH FE simulation models (Design 1 and Design 2) for the industrial bolt in Fig. 1

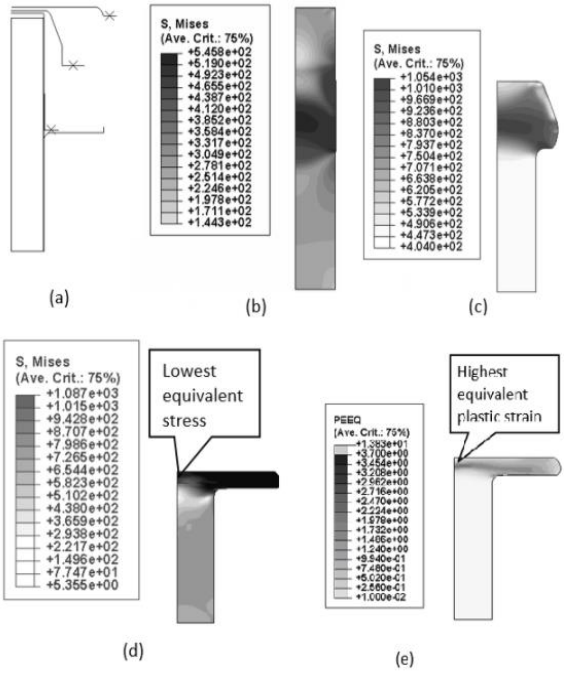

Fig. 12 FE analysis of design one for the three-stage CH of industrial bolt (Design 2): (a) Blank with dies, (b to d) evolution of the equivalent stress, (e) distribution of the equivalent plastic strain at the end of third stage

Fig. 13-a reveals that the highest damage level within the bolt's head at the final stage of heading for both designs using the 1008 steel did not exceed the acceptable limits. Thus, using the 1008 steel in the manufacturing of the industrial bolt using both three stage CH designs will result in an acceptable final product.

Applying the same assessment methodology to the three-stage CH designs using the 1038 steel revealed that the predicted maximum damage levels in the bolt head exceeded acceptable limits, and it will therefore experience internal ductile failure (Fig.13-b).

The workability evaluation of both designs can be used to ascertain the better design that reduces the internal ductile

ISSN (Online) 2456-1290

International Journal of Engineering Research in Mechanical and Civil Engineering (IJERMCE)

Volume 11, Issue 7, July 2024

damage in the cold headed product.

In conclusion, the local equivalent plastic strain and damage levels inside bolts made of medium carbon steels reached high limits due to the strain localization process. On the other hand, lower equivalent plastic strains and damage levels were reached in the bolts made of the low carbon steels.

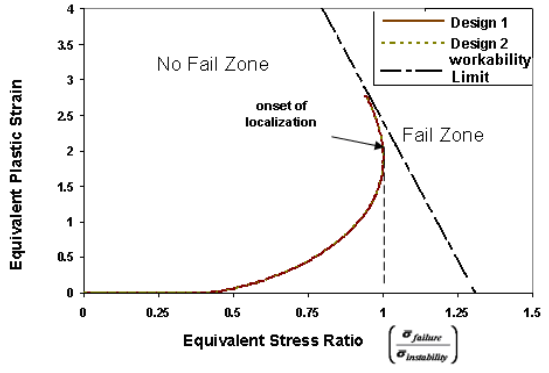

(a)

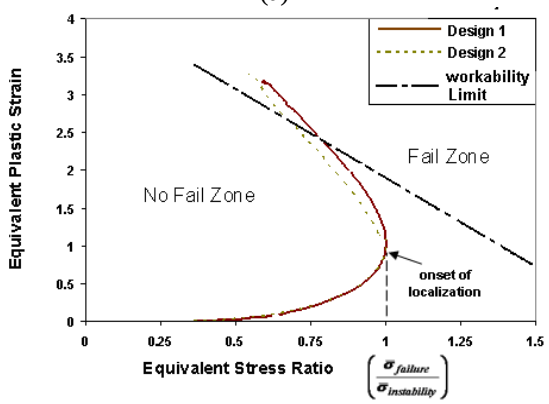

(b)

Fig. 13 Evaluation of three-stage CH designs using the stress instability criterion: (a) 1008 steel, (b) 1038 steel.

IV. CONCLUSIONS

In the multistage CH applications using the three-stage, the stress instability workability criterion was able to capture the local internal ductile failure.

This result indicates that it is possible to use this workability criterion to predict the initiation and location of the internal ductile failure. Also, this workability criterion showed its capability to indicate the differences in the damage levels produced by different multistage CH designs. It can be used to select the CH materials that assure a defect-free cold-headed product.

As a result, this workability criterion presented in this study can be used efficiently to predict the damage levels and failure initiation location inside the ASBs in the cold-headed products and can be used as a design optimization tool to improve the existing design procedures currently based on rules of thumb.

REFERENCES

[1]. A. Sabih, J.A. Nemes, “Internal ductile failure mechanisms in steel cold heading process”, Journal of Materials Processing Technology, vol. 209, Issue 9, pp. 4292-4311, 2009.

[2]. R.J., Clifton, “Adiabatic shear banding. In Material Response to Ultra-High Loading Rates NMAB-356. National Materials Advisory Board (NRC). Washington DC. Ch. 8, pp. 129-142, 1980.

[3]. Y.L. Bai, “Thermo-plastic instability in simple shear”, Journal of the Mechanics and Physics of Solids, vol. 30, Issue 4, pp. 195-207, 1982.

[4]. A.M. Merzer, “Modelling of adiabatic shear band development from small imperfections”, Journal of the Mechanics and Physics of Solids, vol. 30, Issue 5, pp. 323-338, 1982.

[5]. T.W. Wright, and R.C. Batra, “The initiation and growth of adiabatic shear bands”, International Journal of Plasticity, vol. 1, Issue 3, pp. 205-212,1985.

[6]. A. Sabih, J.A. Nemes, “New Stress Instability Workability Criterion for Internal Ductile Failure in Steel Cold Heading Process”, Journal of International Journal of Engineering Research in Mechanical and Civil Engineering (IJERMCE), vol. 10, Issue 10, pp. 46-52, 2023.

[7]. M.A. Meyers, and C.L. Wittman, "Effect of Metallurgical Parameters on Shear Band Formation in Low-Carbon (~0.20 wt. pct.) Steels", Metallurgical Transaction A, vol. 21A, pp. 3153-3164, 1990.

[8]. J.R. Klepaczko, and B. Rezaig, “A numerical study of adiabatic shear banding in mild steel by dislocation mechanics based constitutive relations”, Mechanics of Materials, vol. 24, Issue 2, pp. 125-139, 1996.

[9]. M. Nabil Bassim, “Study of the formation of adiabatic shear bands in steels”, Journal of Materials Processing Technology, vol. 119, Issues 1–3, pp. 234-236, 2001.

[10]. Marchand, and J. Duffy, “An experimental study of the formation process of adiabatic shear bands in a structural steel”, Journal of the Mechanics and Physics of Solids, vol. 36, Issue 3, pp. 251-283, 1988.

[11]. R.C. Batra, and N.M. Wilson, “Adiabatic shear bands in plane strain deformations of a WHA”, International Journal of Plasticity, vol. 14, Issues 1–3, pp. 43-60, 1998.

[12]. R.C. Batra, and M.H. Lear, “Adiabatic shear banding in plane strain tensile deformations of 11 thermoelastoviscoplastic materials with finite thermal wave speed”, International Journal of Plasticity, vol. 21, Issue 8, pp. 1521-1545, 2005.

[13]. Deltort, “Experimental and numerical aspects of adiabatic shear in a 4340 steel”, Journal de Physique IV, France Colloq. vol. 4, pp. 447–452, 1994.

[14]. N. Nickoletopoulos,” Physical and numerical modeling of fracture during Upsetting for Cold Heading Operations”, Doctoral dissertation, McGill University at Montreal, 2000

[15]. G. R. Johnson, and W. H. Cook, “A constitutive model and data for metals subjected to large strains, high strain rates and high temperatures,” In Proceedings of the Seventh International Symposium on Ballistic, pp. 541-547. The Hague, Netherland, 1983.

[16]. T.W. Wright, and J.W. Walter, “On stress collapse in adiabatic shear bands”, Journal of the Mechanics and Physics of Solids, vol. 35, Issue 6, pp. 701-720, 1987.

[17]. M.A. Meyers, G. Subhash, B.K. Kad, and L. Prasad, “Evolution of microstructure and shear-band formation in α-hcp titanium”, Mechanics of Materials, vol .17, Issues 2–3, pp. 175-193, 1994

ISSN (Online) 2456-1290

International Journal of Engineering Research in Mechanical and Civil Engineering (IJERMCE)

Volume 11, Issue 7, July 2024

[18]. G.R. Johnson, and T.J. Holmquist, "Evaluation of cylinder-impact test data for constitutive model constants", Journal of Applied Physics, vol. 64, Issue 8, pp 3901 – 3910, 1988.
[19]. H. Kolsky, "An investigation of the mechanical properties of materials at very high rates of loading," In Proceeding of the Physical Society, section B., vol. 62, pp. 676-700, 1949.